ACS SENSORS

Article

Cite This: ACS Sens. 2018, 3, 2367−2374

pubs.acs.org/acssensors

Emergent Electrical Properties of Ensembles of 1D Nanostructures and Their Impact on Room Temperature Electrical Sensing of Ammonium Nitrate Vapor

Lyndon D. Bastatas, Elena Echeverria-Mora, Phadindra Wagle, Punya Mainali, Aaron Austin, and David N. McIlroy*

Department of Physics, Oklahoma State University, Stillwater, Oklahoma 74078, United States

ABSTRACT: Ammonium nitrate is an explosive agent that has a very low vapor pressure, which makes airborne detection very challenging. Detection of ammonium nitrate vapor has been achieved by using silica nanospring mats coated with a thin semiconducting layer of zinc oxide. The sensor was operated at room temperature and under ambient conditions in air. Lock-in amplification was employed to measure the change in electrical resistance of the sensor upon exposure to the said target gas analyte. The sensor showed fast detection, only taking ∼15 s to reach its peak response, and exhibited a moderate recovery time of approximately 0.5 min/20 ppm for <40 ppm exposures. A comparison between the ZnO coated nanospring sensor and ZnO thin film sensor demonstrated that the nanospring sensor has superior sensitivity and responsiveness over the thin film sensor. A percolation-based model is proposed to explain the greater sensitivity at low analyte concentrations of the ZnO-nanospring sensor, as compared to a ZnO thin film sensor.

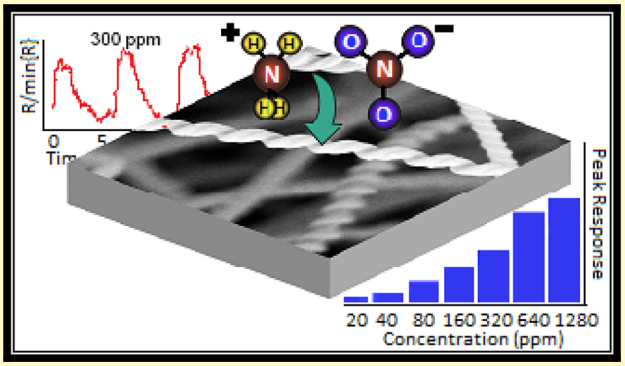

KEYWORDS: *nanospring, gas sensor, ammonium nitrate, percolation model, ZnO, room-temperature operation*

One of the keys to technology has and always will be the ability to quantify and measure. As technology has evolved, so has the need for precision sensors in areas ranging from automation to safety. This is particularly true when it comes to society safety and security. Unfortunately, the use of improvised explosive devices across the globe is motivating the need to develop advanced explosives sensor technology. The list of requirements for the next generation of explosives sensors is very long. Specifically, they should detect in real time; have parts per billion or parts per trillion sensitivity; operate under ambient conditions (atmosphere, temperature, etc.); and be reliable (minimal false positives), reusable, low power consuming, portable, and low cost. Technology exists to detect parts per billion concentrations of explosive residue in the air[1−4] and in liquid;[5−8] the problem is cost and portability. Semiconducting metal oxides are widely used for chemical sensing because their electrical conductivity is highly dependent on their chemical stoichiometry, morphology, surface chemistry, temperature, and responsiveness to light, to name a few.[9−13]

Among the metal oxides, zinc oxide (ZnO) is becoming increasingly popular as a platform for chemical sensing.[14,15] It is normally an n-type semiconductor with a wide and direct band gap and high electron mobility.[16] It is low-cost, nontoxic, and rich in defect chemistry contingent on the processing method and conditioning.[17,18] One model of the gas sensing mechanism suggests that the electrical response of the sensor is determined by the interaction of the target gas analytes and oxygen vacancies at the surface,[19] although simulation studies pointed out that oxygen vacancies in n-type semiconductor are deep level donors under normal conditions.[20] As a chemical sensor, it is typically operated in what is known as a redox mode,[14,21−23] where the oxygen stoichiometry at the surface can be increased or decreased depending on whether it is a reduction or oxidation reaction. In the case of n-type ZnO, and depending on the target gas analyte, a reduction event can occur that reduces the oxygen content at the ZnO surface, thereby causing it to be metal rich with a concomitant increase in electrical conductivity. Upon reoxidation of the ZnO surface, the original conductivity is restored. Consequently, ZnO, as well as other semiconducting metal oxides, are ideally suited for operation in air.

To improve the sensitivity of ZnO as a sensor, it has been constructed with various architectural designs such as p-Si/n-ZnO heterojunctions,[24−26] field effect transistors-type structures,[27] and various nanostructured morphologies including nanowires, nanobelts, and nanosprings, where the argument is that they present more surface in a given volume relative to a planar surface, ergo more surface sites with which the target analyte can react.[28−31] However, the argument that increasing the surface area will increase the sensitivity of a sensor is

Received: July 30, 2018
Accepted: October 23, 2018
Published: October 23, 2018

DOI: 10.1021/acssensors.8b00746
ACS Sens. 2018, 3, 2367−2374

inconsistent with the fundamentals of sensing based on the following argument:

The change in resistance (ΔR) of a chemical sensor is a function of the number density of sites accessible to the analyte (N) and the concentration of the analyte (N_A). If one assumes 100% efficiency of the reaction of the analyte with the sensor surface, it is simple to show that the fractional change in the resistance is given by the following relationship:

$$\frac{\Delta R}{R_o} \propto \frac{N_A}{N} \quad (1)$$

where R_o is the initial resistance. On the basis of eq 1, we do not expect sensors constructed with high surface area materials to be responsive at low concentrations of the target analyte, but time and again, it has been demonstrated that high surface area nanostructured ZnO chemical sensors exhibit greater sensitivity at lower analyte concentrations than their thin film counterparts.[32] The only way to circumvent this obvious contradiction of greater surface area producing higher sensitivity is that a very small number of analyte reactions can produce extremely large responses. This contradiction is one of the topics of discussion of this study.

One downside of ZnO of redox based chemical sensors, regardless of morphology, is that a good signal-to-noise ratio at low analyte concentrations requires operation at temperatures in excess of 200 °C,[33−37] which leads to the second downside of redox chemical sensors. Redox chemical sensors lack selectivity, glaringly so when compared to spectroscopic detection,[38] because the analyte is physically altered. In fact, the detection of a reactive compound within the gas stream occurs, thereby producing false positive detection. While metal oxide redox-based chemical sensors are well suited for highly controlled environments, such as an oxygen sensor in an automobile, they are less suitable for use in uncontrolled environments.

The well-accepted approach for introducing selectivity to an electrically based chemical sensor, regardless of their chemical composition, is surface functionalization with a receptor that exclusively targets the analyte in question. Unfortunately, identifying promising surface functional groups that are stable at or above 200 °C is quite challenging. Consequently, one must reconsider redox-based detection in favor of selective surface adsorption. This is a challenging proposition because the sensor response will be a function of subtle charge redistribution, i.e., a field effect driven response. Furthermore, room temperature (RT) operation is safer and more practical, although, as a drawback, the target analyte must compete with moisture and O_2 for adsorption sites.[22] This hinders the detection capabilities of the sensors, making room temperature gas detection extremely difficult.

Because the goal of the present work is to develop an airborne sensor platform capable of detecting ammonium nitrate (AN), room temperature operation is critical to the integration of molecular receptors of AN. While AN has beneficial uses, e.g., as agricultural fertilizer and oxidizer in air generators and propellants,[39] it is too often exploited as the explosive agent in improvised explosive devices (IED). However, detecting AN is challenging because it has an extremely low vapor pressure.[40] To the best of our knowledge, there are only a few studies of the electrical detection of AN. Chu et al. performed conductometric sensing of AN via redox, where the sensor was operated above 110 °C.[41] Kamonsawas et al. developed a RT polymer sensor capable of detecting 337 ppm of AN;[42] however, the sensor required flushing with N_2 prior to introducing AN. While scientifically interesting, the inability of the sensor to operate in air limits its usefulness, particularly for detection of AN-based IEDs.

Herein, we report on room temperature electrical detection of ammonium nitrate. The sensor utilizes an ensemble of ZnO coated 1D nanostructures and lock-in amplification to detect low parts per million concentrations of AN vapor.[43] Note that because the sensor relies on adsorption, as opposed to chemisorption, its response is due to changes in the surface electric field; ergo, it is a field effect sensor. In addition, we introduce a percolation model we have developed to explain the greater sensitivity of the 1D nanostructure ensemble relative to a planar sensor architecture. Our model resolves the contradiction described above (eq 1) and explains the emergent electrical sensing capabilities of ensembles of 1D nanostructures.

SENSOR FABRICATION

Mats of silica nanospring (NS) were grown on a silicon wafer via a vapor−liquid−solid method that is discussed in detail in references herein.[31,44,45] Briefly, a 15 nm layer of gold was sputtered onto a clean Si substrate with a thick thermal oxide, where the Au was the metal catalyst for nanospring formation. The Au sputtered substrate was placed in a custom-built reactor, where it was heated to approximately 370 °C and exposed at atmospheric pressure to a mixture of N_2, O_2, and a proprietary precursor for approximately 1 h.

Bare silica NSs are electrical insulators, so they will not respond to exposures to gas analytes of any kind. To employ them as chemiresistors, the NS mats were coated with a thin layer of ZnO via atomic layer deposition (ALD) using an OKyay Tech ALD (Turkey) system. The nanosprings were plasma treated for 1 min prior to deposition of ZnO. In performing the ALD, DI water and diethylzinc (Strem Chemicals Inc., >95%) were sequentially introduced inside the reactor chamber for 100 cycles with N_2 as the carrier gas. The chamber was purged with N_2 between every dosing of water and diethylzinc to eliminate residual reactants. The chamber was maintained at 180 °C, with a baseline pressure of ∼200 mTorr. Blank Si wafers were run in parallel with the NS samples for film thickness calibration. Following the above procedure, a 20-nm-thick ZnO layer on the Si wafer was obtained, as determined by ellipsometry (J.A. Woollam, Nebraska). They were subsequently used as ZnO thin film sensors with the purpose of comparing their responsiveness with that of the ZnO-NS sensors.

The ZnO-coated silica nanosprings (ZnO-NS) sensors were postannealed in air for 5 min at 500 °C to optimize their responsiveness to ammonium nitrate. We observed that as-prepared sensors (not annealed) were highly conductive, and their response was highly unstable with poor signal-to-noise. The instability of their electrical response is due to high concentrations of defects because of low ALD deposition temperature. We attribute this to higher than expected conductivity and the small grain size (<10 nm) of the polycrystalline coating, which is prone to structural instability.[46] Annealing heals ZnO defects[47] and induces grain growth,[48] with a caveat: Extended annealing for results in larger grain sizes that exceed the range for optimal sensor responsiveness of ZnO-NS sensors.[49]

DOI: 10.1021/acssensors.8b00746
ACS Sens. 2018, 3, 2367−2374

Figure 1 shows the SEM and TEM images of a ZnO-NS after annealing for 5 min at 500 °C in air. The mat is a network

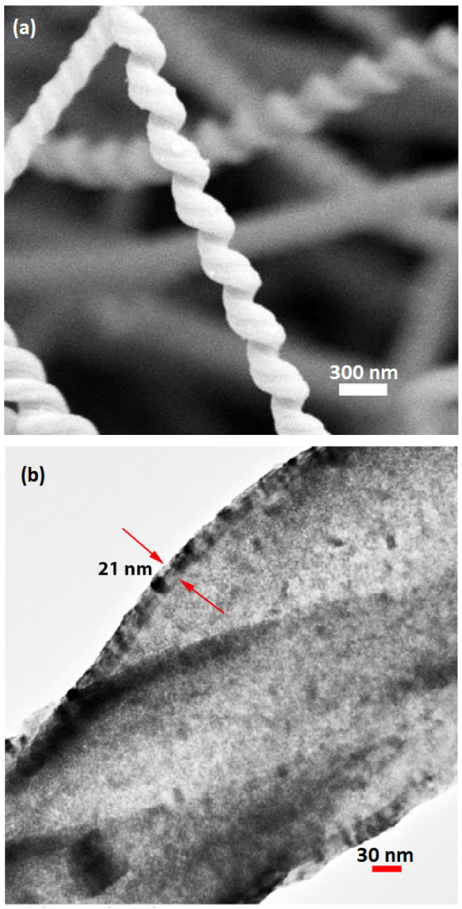

Figure 1. (a) Scanning electron microscopy (SEM) image of ZnO-coated nanospring mat. (b) Transmission electron microscopy (TEM) image of the ZnO grains on a nanospring. The root-mean-square of the grain size correlates with the film thickness.

of interconnected nanosprings with an accessible surface area of 200 m^2/g when coated with ZnO. The high magnification SEM and TEM images reveal that the ZnO grain size is 10−30 nm, which produces a ZnO-NS sensor with a few MΩ resistance. We note that the size of the ZnO nanocrystals dictates the thickness of the coating, where the number of ALD cycles controls the average nanocrystal size, ergo, the thickness of the coating. Furthermore, the sensitivity of the sensor is highly dependent upon the grain size of the crystal. Our previous study found that this range of grain size optimizes the sensor response.[49]

EXPERIMENTAL APPARATUS AND PROCEDURE

The schematic of the sensor test station is displayed in Figure 2. Vaporized AN (Sigma-Aldrich, 98% purity), the analyte, was produced by heating a 125 mL filter flask containing AN powder to 140−170 °C, which produced various vapor concentrations with corresponding vapor temperatures ranging from 80 to 100 °C in the flask. Controlled exposure of the ZnO-NS sensor to AN vapor was achieved by opening and closing a Teflon valve connected to a tee to the carrier gas (dry, clean, air). Note that Teflon tubing was used throughout to mitigate AN vapor from sticking to the gas delivery lines. The carrier gas velocity was held at ∼30 m/s in order to draw the AN vapor from the flask via a weak Venturi effect. The sensor was placed approximately 2 cm away from the outlet of the tube and oriented parallel to the direction of gas flow. The sensor stage consisted of a glass slide upon which stainless steel alligator clips were glued 2 mm apart. The lower jaws of the clips were removed to prevent conduction along the backside of the sensor substrate. To ensure a good contact to the ZnO-NS sensor, indium beads were placed between the clip and the surface of the sensor. The electrical character of the sensor was determined by measuring the current−voltage (I−V) relationship at room temperature and dark conditions using a Keithley meter (not shown). The I−V curve of the sensor when swept from −2 V to +2 V is linear and indicative of good Ohmic contacts. All experiments were conducted at room temperature and under ambient atmospheric conditions. A lock-in amplifier (Stanford Research 510) was used to measure the sensor response with a 90 kHz modulation. The sensor output was fed into a data logger. The sensor was stabilized for a minimum of 30 min prior to data acquisition.

ZnO-NS SENSOR CHARACTERIZATION AND RESPONSE TO AMMONIUM NITRATE

Sensor Baseline Characterization: Thermal and Humidity Response of ZnO-Nanospring Sensor. Because the goal of the study is to develop an electronic ammonium nitrate sensor that can operate under ambient conditions. Consequently, it is necessary to evaluate the sensors' responsiveness to humidity and temperature fluctuations and to set a baseline, which will assist with identifying false positives, and is particularly important for a semiconductor based sensor operated at room temperature. Furthermore, water molecules can compete with AN for surface sites.[22]

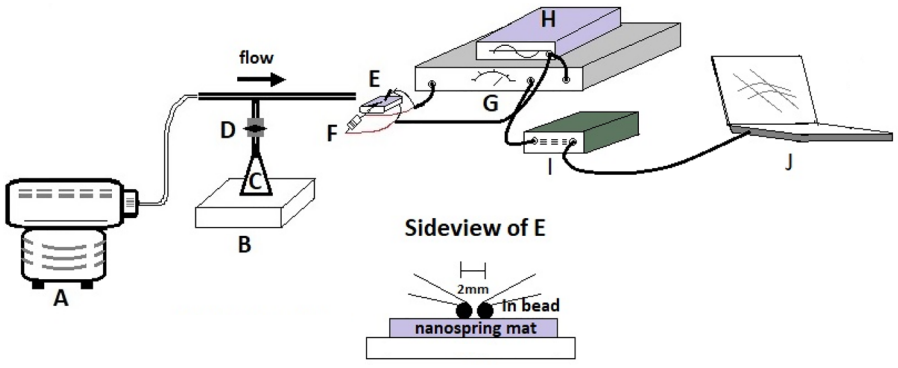

Figure 2. Schematics of the gas sensing setup consisting of (A) air compressor, (B) hot plate, (C) filter flask containing ammonium nitrate, (D) solenoid valve, (E) nanospring mat sensor, (F) resistor, (G) lock-in amplifier, (H) function generator, and (I) data acquisition system which is controlled by the (J) computer.

DOI: 10.1021/acssensors.8b00746
ACS Sens. 2018, 3, 2367−2374

Water vapor was produced by heating DI water to boiling, where the response of the sensor was measured using the same setup presented in Figure 2 ("ON" in the figure indicates that the valve was opened to introduce the vapor). The thermal response of the sensor was obtained by adjusting a substrate heater upon which the sensor was mounted. The temperature of the sensor was monitored using a thermocouple attached to the sensor. Displayed in Figure 3a is the RT change of

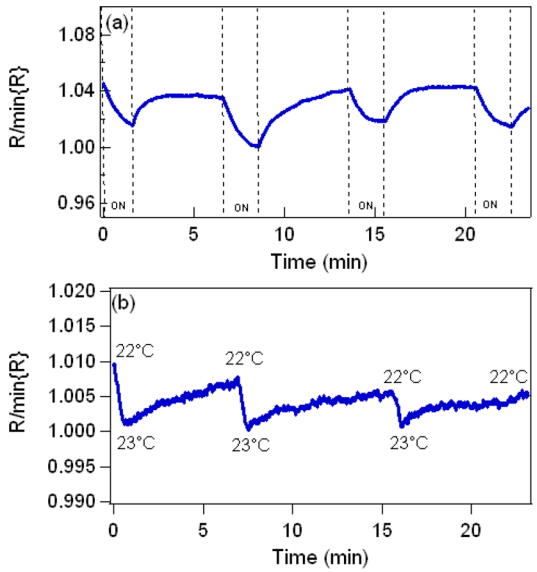

Figure 3. Change of resistivity of ZnO-coated silica nanosprings when (a) exposed to vapor from boiling DI water and (b) a 1 °C temperature change.

resistance of the ZnO-NS sensor to pulses of water vapor. The characteristic response of the sensor to water vapor/moisture is a decrease in resistance. For the water vapor/moisture used to collect data in Figure 3a, a decrease in resistance of approximately 2.5% was observed. The response of the sensor to small changes in temperature is displayed in Figure 3b, where a 1 °C increase in temperature from 22 to 23 °C produced a drop in resistivity of approximately 0.4%. Such a change in resistance is the typical temperature dependent response of a semiconductor. To summarize, the resistance of the ZnO-NS sensor decreases with either moisture or increasing temperature.

Ammonium Nitrate Detection. The response of the ZnO-NS sensor to AN exposure is an increase in the resistance, where the magnitude depends on the AN concentration. A typical example of the sensor's response to a sequence of AN exposures of 300 ppm is displayed in Figure 4a. Note that AN increases the resistance, as opposed to water vapor (Figure 3a) and a temperature change (Figure 3b), where the resistance decreases. The ZnO-NS response to 300 ppm of AN is small at 0.5% above the baseline, even with lock-in detection.

The sensing mechanism of the ZnO-NS sensor for detecting ammonium nitrate in a low humidity environment is as follows.[14−16,21,22] By operating the sensor in an ambient atmosphere, a stabilized surface is maintained, where O_2 can bond to favorable surface defects. This, in conjunction with the applied bias, produces a stable space-charge region at the ZnO surface and concomitant barrier height. The self-refreshing character of the sensor displayed in Figure 4a is an indication

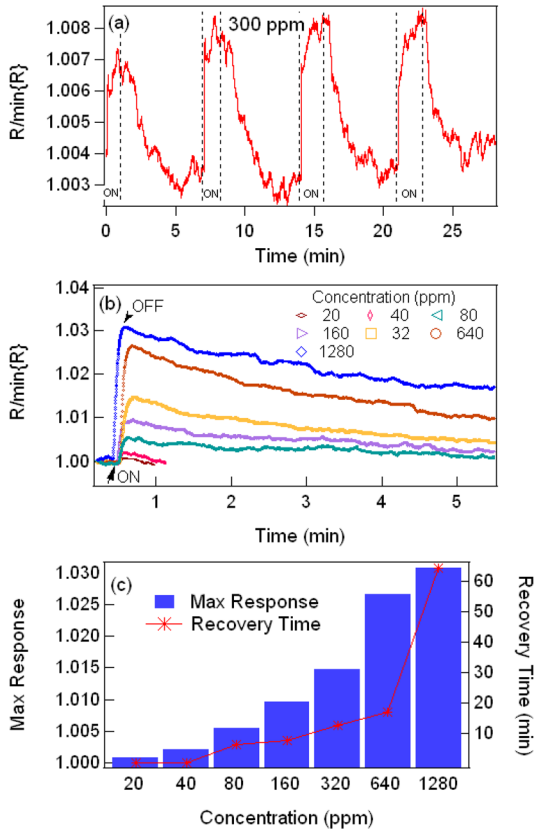

Figure 4. (a) A time sequence response of the ZnO-coated silica nanospring sensor with exposure to 300 ppm AN, (b) the electrical responses and relaxations of the sensor for a single shot exposure to AN at different AN concentrations, and (c) a plot of the maximum responses and recovery times as a function of AN concentration. All the data were collected at room temperature and in an ambient air atmosphere.

of AN physisorbed onto the surface of the ZnO-NS sensor, as opposed to chemisorption associated with a redox reaction. Physisorption on AN is due to dipole−dipole interactions between the dipole moment of AN and an induced dipole at the ZnO surface, e.g., van der Waal forces. The dipole field of AN modulates the surface depletion layer, which in turn affects the overall conductance of the sensor.[50] Therefore, the response of the ZnO-NS sensor operated at room temperature is that of a field effect sensor.

The recovery of the sensor (self-refreshing) as a function of AN concentration is displayed in Figure 4b and has the characteristic double exponential decay typical of metal oxide sensors.[51] We have designated recovery to be the return of the resistance to within 10% of the baseline. The recovery of the sensor as a function of AN concentration using this criterion is plotted in Figure 4c. Included in Figure 4c is the maximum response of the sensor as a function of AN concentration. Both the recovery and maximum response fit a log-normal function, indicating that both processes have a maximum entropy probability distribution. This is consistent with our analysis of single ZnO-NS redox sensors.[32] Identification of maximum entropy probability distribution is important to modeling the response and sensitivity of ZnO-NS sensors discussed in the Percolation Theory of ZnO-NS Sensor Responsiveness section.

DOI: 10.1021/acssensors.8b00746
ACS Sens. 2018, 3, 2367−2374

To differentiate the performance of the ZnO-NS sensor with that of a ZnO thin film (ZnO-TF) sensor, both sensing platforms were dosed with low and high concentrations of vaporized AN. Figure 5a is the room temperature response of

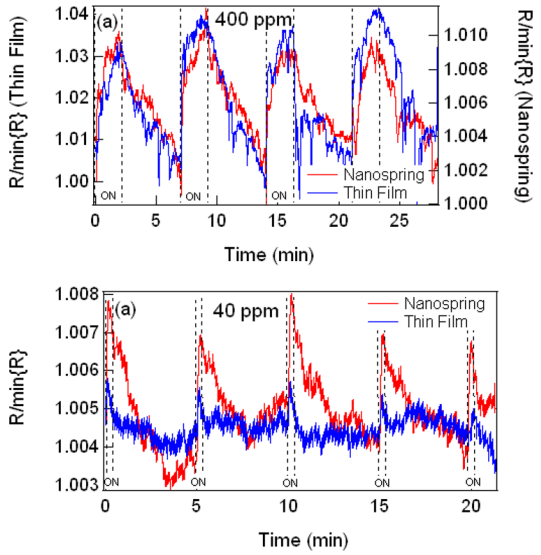

Figure 5. A comparison of the change in electrical resistance of ZnO-coated silica nanospring mats and ZnO thin film sensors with (a) 400 ppm concentration of AN and (b) 40 ppm concentration of AN.

the ZnO-NS and ZnO-TF sensors to 400 ppm of AN. The ZnO-NS sensor response is slightly larger than that of the ZnO-TF sensor, but not significantly. However, it is interesting to note that when these two sensors are operated at high temperature, in a redox mode, and at high analyte (toluene) concentrations, the ZnO-TF sensor response is significantly higher than that of the ZnO-NS sensor.[32] Displayed in Figure 5b is the response of the sensors to 40 ppm of AN. Upon examination, it can be seen that the ZnO-NS is much more responsive than the ZnO-TF sensor, again, consistent with previous work.[32] The ultimate low detection limit of the sensors, which is defined as the lowest concentration at which the response is comparable to the noise, is 20 and 35 ppm for ZnO-NS and ZnO-TF sensors, respectively.

To better understand the enhanced sensitivity of ZnO-NS sensors, Bakharev et al. studied and modeled the toluene redox sensing of a ZnO-NS sensor constructed from a single nanospring,[32] where it was found that the periodic boundary conditions of the nanospring resulted in greater sensitivity due to finite size screening. The model also effectively predicted the concentration dependent trends of a thin film and the nanospring sensor. While this study illuminates the effects of finite size on electron screening in a single nanospring, by itself, it is insufficient for explaining the increased sensitivity of a sensor constructed with an ensemble of ZnO-NS. However, we will demonstrate that through the application of percolation theory, the superior sensitivity of the ZnO-NS sensor over that of the ZnO-TF sensor can be understood.

PERCOLATION THEORY OF ZnO-NS SENSOR RESPONSIVENESS

The superior sensitivity of the ZnO-NS sensor over the ZnO-TF sensor in Figure 5 contradicts eq 1, which states that the response of a sensor with a large number of receptors (larger surface area) will be less responsive than one with fewer receptors. The equivalent circuit of the sensors in this study, be they NS or TF, can be modeled as a random network of interconnected resistors. The adsorption of AN at or near a preferred pathway of least resistance increases the resistance, where the effect is that said pathway is no longer one of multiple equivalent paths of least resistance within the network. Because the number of "resistors" in the sensors are finite, they will eventually become saturated with AN, at which point the network reaches a critical concentration of dead conduction pathways (pc) that render it nonconductive.

We propose that within the three-dimensional ZnO-NS network there are junctions between nanosprings (Figure 1a), where we define a junction as points of contact between two or more NS, that are critical to the conductivity of the system. Note that the said junctions do not exist in a two-dimensional TF. Furthermore, we argue that there are large clusters of NS interconnected through these critical junctions. We postulate that these junctions operate along the principle of a field effect transistor, such that they regulate the flow of current, where the electric field of the adsorbed analyte modulates the conductivity. The clusters become isolated from one another, or interact minimally, when conduction through the junctions is deactivated. Upon deactivation, large regions of the NS network are isolated and no longer participate in the conduction of current. Consequently, a few junctions dominate the conductivity of the network, which we will call super junctions. We hypothesize that the density of these super junctions is on the order of hundreds of parts per million. The net effect the super junctions have on the NS network is that at high analyte concentrations, the NS sensor is less responsive and less dynamic to small changes in the analyte concentration, which is what we observed in this and previous studies.[32] However, we propose that these super junctions are also responsible for the low detection limit of the ZnO-NS sensor relative to the ZnO-TF sensor. Regardless of the sensing mechanism, a sensor constructed with 1D nanostructures or a thin film (2D) can be modeled using percolation theory and the motivation for employing it here.

In the context of percolation theory, conductance ($G_{TF}(\rho)$) of a two-dimensional random resistive network, such as a nanocrystalline ZnO thin film, follows a power law:

$$G_{TF}(p) \propto (p - p_c)^t \tag{2}$$

where p is the fraction of conductive sites in the network, p_c is the critical concentration at which the network is no longer conductive, and t is a critical exponent that describes the mathematical dimensionality of the network.[52] It has been shown that $t \approx 1.3$ is an appropriate value for a 2D lattice and in the range $0.3 < t < 0.4$ for a 3D lattice.[53,54] The critical concentration (p_c) of a 2D percolative network is 0.5, and the conductance is

$$G_{TF}(p) \propto (p - 0.5)^{1.3} \tag{3}$$

Eq 3 can be applied to the ZnO-TF sensor, but not to the ZnO-NS sensor. However, the ZnO coating on the NS is a 2D nanocrystalline coating, and therefore, eq 3 does describe the conductance in a single ZnO-NS in the context of percolation theory, which will be used in the development of the full percolative model of the conductance of the ZnO-NS sensor.

A random network of 1D nanostructures, such as nanosprings, is a 3D percolative network. However, Kumar et al.

DOI: 10.1021/acssensors.8b00746
ACS Sens. 2018, 3, 2367−2374

found that the conduction in a quasi-3D array of carbon nanotubes is best described as a 2D percolating network.[55] We argue that because of the high degree of overlapping of nanosprings and the subsequent directional changes of the current (forward and backward relative to the electrode bias), etc., the critical exponent is neither purely 2D nor 3D. We propose that $1.3 < t < 2$ is appropriate for the NS network, where the upper limit is consistent with the findings of Martin et al. for cross-linked chains.[56] It is more difficult to define p_c for a 3D percolative network of NS. However, a crude estimate is made by assuming that p_c is the volume fraction of NS contained within the network. The volume fraction of nanosprings is 2%, or $p_c = 0.02$. While extremely small, this value accounts for the much higher degree of interconnectedness in a 3D network compared to a 2D network. Note that $p_c = 0.02$ is likely much larger than is the case in the ensemble of NS, but serves as a good starting point for developing a percolation model for an ensemble of 1D nanostructures. If we ignore the nanocrystalline morphology of the ZnO coating on the NS and instead treat them as single crystal ZnO nanowires (NW), the conductance (G_{NW}) is defined by

$$G_{NW}(p') \propto (p' - 0.02)^2 \tag{4}$$

where p' is the number of critical 1D nanowire junctions within the ensemble and the choice of critical exponent is based on the work by Martin et al.[56] This applies to a nanospring network but is incomplete. The nanocrystal morphology of the ZnO coating on the surface of the NS adds a second level of disorder and is an independent variable (A_{NC}). Consequently, the probability of conduction, P_r, is the product of the probability of conduction through the nanocrystal ZnO network of each nanospring, $P_r(A_{NC})$, and through the 1D nanostructured network, $P_r(A_{NW})$, or $P_r(A_{NC} \cap A_{NW})$. The conductance is then the product of eqs 3 and 4

$$G_{NS}(p, p') \propto G_{TF}(p) \cap G_{NW}(p') \propto (p - 0.5)^{1.3}(p' - 0.02)^2 \tag{5}$$

Therefore, the conductance through the network is the product of that of a thin film and a network of 1D nanostructures. If we assume that $p' \sim p_c$ (= 0.02), then G_{NW} dominates eq 5. We can use eqs 3 and 5 to calculate the normalized change in conductance of the NS network and the TF as a function of p and p'. Taking the derivative of eq 3 with respect to p and dividing by eq 3, we obtain the following relationship for the normalized change in conductance of a thin film:

$$\frac{dG_{TF}}{G_{TF}} = \frac{1.3}{p - 0.5}dp \tag{6}$$

Doing the same for eq 5 yields

$$\frac{dG_{NS}}{G_{NS}} = \frac{1.3}{p - 0.5}dp + \frac{2}{p' - 0.02}dp' \tag{7}$$

At high analyte concentrations, we see that eq 7 yields a normalized change in conductance similar to that of a thin film (eq 6) because the second term in eq 7 is saturated and $dp' \approx 0$. However, for very small analyte concentrations, the thin film term is essentially a constant. For $p' \sim p_c$ (= 0.02), the second term dominates eq 7 even though the term is small. This is consistent with the results in Figure 5b, where at low AN concentrations, the normalized change in resistance for the ZnO-NS sensor is much larger than that of the ZnO-TF sensor. While eq 7 cannot completely describe the response of the ZnO-NS sensor, it captures the essentials and statistical nature of the sensor and elucidates the effects of morphology on sensor performance. Furthermore, it supports our hypothesis of the presence of super junctions within the NS network of the ZnO-NS sensor and that they control the conductivity and are responsible for its sensitivity to low exposures to ammonium nitrate. Last, eq 7 explains why the nanospring-based sensor supersedes the limitations set by eq 1.

SUMMARY AND CONCLUSION

We have demonstrated, with the aid of lock-in amplification, that ZnO-coated silica nanospring sensors are capable of detecting ammonium nitrate vapor at 40 ppm when operated at room temperature and in an ambient air atmosphere. The ZnO-NS sensor responded quickly and with a moderate recovery rate. The electrical resistance of the sensor increases upon exposure to the said analyte and the opposite response to water vapor or a slight increase in temperature. We also demonstrated that the ZnO-NS is more sensitive at low AN concentrations than a ZnO-TF sensor. Finally, we have demonstrated that percolation theory can be used to model the ZnO-NS and ZnO-TF sensors. The success of the model supports our conclusion that the superior response of the ZnO-NS sensor to low exposures of AN is due to the presence of super junctions that significantly impact the conductivity of the sensor; i.e., a small number of AN adsorption events produce significant changes in the sensors response.

AUTHOR INFORMATION

Corresponding Author

*E-mail: dave.mcilroy@okstate.edu.

ORCID

Lyndon D. Bastatas: 0000-0003-1199-9676

Notes

The authors declare no competing financial interest.

ACKNOWLEDGMENTS

D.N.M. would like to acknowledge the support of the Office of Naval Research (N00014-17-1-2593).

ABBREVIATIONS

AN, ammonium nitrate; IED, improvised explosive devices; RT, room temperature; NS, nanospring; TF, thin film

REFERENCES

(1) Naddo, T.; Che, Y.; Zhang, W.; Balakrishnan, K.; Yang, X.; Yen, M.; Zhao, J.; Moore, J. S.; Zang, L. Detection of explosives with a fluorescent nanofibril film. *J. Am. Chem. Soc.* **2007**, *129*, 6978−6979.

(2) Liu, Y.; Mills, R. C.; Boncella, J. M.; Schanze, K. S. Fluorescent polyacetylene thin film sensor for nitroaromatics. *Langmuir* **2001**, *17*, 7452−7455.

(3) Collin, W. R.; Serrano, G.; Wright, L. K.; Chang, H.; Nuñovero, N.; Zellers, E. T. Microfabricated gas chromatograph for rapid, trace-level determinations of gas-phase explosive marker compounds. *Anal. Chem.* **2014**, *86*, 655−663.

(4) Mullen, C.; Irwin, A.; Pond, B. V.; Huestis, D.; Coggiola, M. J.; Oser, H. Detection of Explosives and Explosives-Related Compounds by Single Photon Laser Ionization Time-of-Flight Mass Spectrometry. *Anal. Chem.* **2006**, *78*, 3807−3814.

DOI: 10.1021/acssensors.8b00746
ACS Sens. 2018, 3, 2367−2374

(5) Saha, S.; Mandal, M. K.; Chen, L. C.; Ninomiya, S.; Shida, Y.; Hiraoka, K. Trace level detection of explosives in solution using leidenfrost phenomenon assisted thermal desorption ambient mass spectrometry. *Mass Spectrom.* **2013**, *2*, S0008.
(6) Primera-Pedrozo, O. M.; Jerez-Rozo, J. I.; De La Cruz-Montoya, E.; Luna-Pineda, T.; Pacheco-Londoño, L. C.; Hernández-Rivera, S. P. Nanotechnology-based detection of explosives and biological agents simulants. *IEEE Sens. J.* **2008**, *8*, 963−973.
(7) Hrapovic, S.; Majid, E.; Liu, Y.; Male, K.; Luong, J. H. T. Metallic nanoparticle-carbon nanotube composites for electrochemical determination of explosive nitroaromatic compounds. *Anal. Chem.* **2006**, *78*, 5504−5512.
(8) Marple, R. L.; LaCourse, W. R. A platform for on-site environmental analysis of explosives using high performance liquid chromatography with UV absorbance and photo-assisted electrochemical detection. *Talanta* **2005**, *66*, 581−590.
(9) Batzill, M.; Diebold, U. The surface and materials science of tin oxide. *Prog. Surf. Sci.* **2005**, *79*, 47−154.
(10) Choi, K. J.; Jang, H. W. One-dimensional oxide nanostructures as gas-sensing materials: Review and issues. *Sensors* **2010**, *10*, 4083−4099.
(11) Korotcenkov, G. Gas response control through structural and chemical modification of metal oxide films: state of the art and approaches. *Sens. Actuators, B* **2005**, *107*, 209−232.
(12) Comini, E. Metal oxide nano-crystals for gas sensing. *Anal. Chim. Acta* **2006**, *568*, 28−40.
(13) Fine, G. F.; Cavanagh, L. M.; Afonja, A.; Binions, R. Metal oxide semi-conductor gas sensors in environmental monitoring. *Sensors* **2010**, *10*, 5469−5502.
(14) Tiwale, N. Zinc oxide nanowire gas sensors: fabrication, functionalisation and devices. *Mater. Sci. Technol.* **2015**, *31*, 1681−1697.
(15) Ahmad, M.; Zhu, J. ZnO based advanced functional nanostructures: synthesis, properties and applications. *J. Mater. Chem.* **2011**, *21*, 599−614.
(16) Özgür, Ü.; Alivov, Y. I.; Liu, C.; Teke, A.; Reshchikov, M. A.; Doğan, S.; Avrutin, V.; Cho, S.-J.; Morkoç, H. A comprehensive review of ZnO materials and devices. *J. Appl. Phys.* **2005**, *98*, 041301.
(17) Schmidt-Mende, L.; MacManus-Driscoll, J. L. ZnO - nanostructures, defects, and devices. *Mater. Today* **2007**, *10*, 40−48.
(18) Janotti, A.; Van De Walle, C. G. Native point defects in ZnO. *Phys. Rev. B: Condens. Matter Mater. Phys.* **2007**, DOI: 10.1103/PhysRevB.76.165202.
(19) Gurlo, A.; Riedel, R. In situ and operando spectroscopy for assessing mechanisms of gas sensing. *Angew. Chem., Int. Ed.* **2007**, *46*, 3826−3848.
(20) Janotti, A.; Van de Walle, C. G. Fundamentals of zinc oxide as a semiconductor. *Rep. Prog. Phys.* **2009**, *72*, 126501.
(21) Tricoli, A.; Righettoni, M.; Teleki, A. Semiconductor gas sensors: dry synthesis and application. *Angew. Chem., Int. Ed.* **2010**, *49*, 7632−7659.
(22) Zhu, L.; Zeng, W. Room-temperature gas sensing of ZnO-based gas sensor: A review. *Sens. Actuators, A* **2017**, *267*, 242−261.
(23) Miller, D. R.; Akbar, S. A.; Morris, P. A. Nanoscale metal oxide-based heterojunctions for gas sensing: A review. *Sens. Actuators, B* **2014**, *204*, 250−272.
(24) Hoffmann, M. W. G.; Mayrhofer, L.; Casals, O.; Caccamo, L.; Hernandez-Ramirez, F.; Lilienkamp, G.; Daum, W.; Moseler, M.; Waag, A.; Shen, H.; Prades, D. A highly selective and self-powered gas sensor via organic surface functionalization of p-Si/n-ZnO diodes. *Adv. Mater.* **2014**, *26*, 8017−8022.
(25) Wang, Z.; Yu, R.; Wang, X.; Wu, W.; Wang, Z. L. Ultrafast Response p-Si/n-ZnO Heterojunction Ultraviolet Detector Based on Pyro-Phototronic Effect. *Adv. Mater.* **2016**, *28*, 6880−6886.
(26) Li, X.; Liang, R.; Tao, J.; Peng, Z.; Xu, Q.; Han, X.; Wang, X.; Wang, C.; Zhu, J.; Pan, C.; Wang, Z. L. Flexible Light Emission Diode Arrays Made of Transferred Si Microwires-ZnO Nanofilm with Piezo-Phototronic Effect Enhanced Lighting. *ACS Nano* **2017**, *11*, 3883−3889.
(27) Feng, P.; Shao, F.; Shi, Y.; Wan, Q. Gas Sensors Based on Semiconducting Nanowire Field-Effect Transistors. *Sensors* **2014**, *14*, 17406−17429.
(28) Wan, Q.; Li, Q. H.; Chen, Y. J.; Wang, T. H.; et al. Fabrication and ethanol sensing characteristics of ZnO nanowire gas sensors. *Appl. Phys. Lett.* **2004**, *84*, 3654−3656.
(29) Wang, J. X.; Sun, X. W.; Yang, Y.; Huang, H.; Lee, Y. C.; Tan, O. K.; Vayssieres, L. Hydrothermally grown oriented ZnO nanorod arrays for gas sensing applications. *Nanotechnology* **2006**, *17*, 4995−4998.
(30) Ding, Y.; Wang, Z. L. Structures of planar defects in ZnO nanobelts and nanowires. *Micron* **2009**, *40*, 335−342.
(31) McIlroy, D. N.; Alkhateeb, A.; Zhang, D.; Aston, D. E.; Marcy, A. C.; Norton, M. G. Nanospring formation—unexpected catalyst mediated growth. *J. Phys.: Condens. Matter* **2004**, *16*, R415−R440.
(32) Bakharev, P. V.; McIlroy, D. N. The effect of the periodic boundary conditions of a ZnO-coated nanospring on its surface redox-induced electrical response. *Nanotechnology* **2014**, *25*, 475501.
(33) Dobrokhotov, V.; Oakes, L.; Sowell, D.; Larin, A.; Hall, J.; Barzilov, A.; Kengne, A.; Bakharev, P.; Corti, G.; Cantrell, T.; Prakash, T.; Williams, J.; Bergman, L.; Huso, J.; McIlroy, D. N. Thermal and optical activation mechanisms of nanospring-based chemiresistors. *Sensors* **2012**, *12*, 5608−5622.
(34) Dobrokhotov, D.; Oakes, L.; Sowell, D.; Larin, A.; Hall, J.; Kengne, A.; Bakharev, P.; Corti, G.; Cantrell, T.; Prakash, T.; Williams, J.; McIlroy, D. N. Toward the nanospring-based artificial olfactory system for trace-detection of flammable and explosive vapors. *Sens. Actuators, B* **2012**, *168*, 138−148.
(35) Chang, J.; Ahmad, M. Z.; Wlodarski, W.; Waclawik, E. R. Self-assembled 3D ZnO porous structures with exposed reactive {0001} facets and their enhanced gas sensitivity. *Sensors* **2013**, *13*, 8445−8460.
(36) Cho, P.-S.; Kim, K.-W.; Lee, J.-H. NO2 sensing characteristics of ZnO nanorods prepared by hydrothermal method. *J. Electroceram.* **2006**, *17*, 975−978.
(37) Park, J. A.; Moon, J.; Lee, S. J.; Kim, S. H.; Chu, H. Y.; Zyung, T. SnO2-ZnO hybrid nanofibers-based highly sensitive nitrogen dioxides sensor. *Sens. Actuators, B* **2010**, *145*, 592−595.
(38) Liu, X.; Cheng, S.; Liu, H.; Hu, S.; Zhang, D.; Ning, H. A Survey on Gas Sensing Technology. *Sensors* **2012**, *12*, 9635−9665.
(39) Oommen, C.; Jain, S. R. Ammonium nitrate: A promising rocket propellant oxidizer. *J. Hazard. Mater.* **1999**, *67*, 253−281.
(40) Brandner, J. D.; Junk, N. M.; Lawrence, J. W.; Robins, J. Vapor Pressure of Ammonium Nitrate. *J. Chem. Eng. Data* **1962**, *7*, 227−8.
(41) Chu, Y.; Mallin, D.; Amani, M.; Gregory, O. J. Detection of explosives using orthogonal gas sensors. *IEEE Sens.* **2013**, 1−4.
(42) Kamonsawas, J.; Sirivat, A.; Niamlang, S.; Hormnirun, P.; Prissanaroon-Ouajai, W. Electrical conductivity response of poly-(Phenylene-vinylene)/ zeolite composites exposed to ammonium nitrate. *Sensors* **2010**, *10*, 5590−5603.
(43) Bakharev, P. V.; McIlroy, D. N. Signal-to-noise enhancement of a nanospring redox-based sensor by lock-in amplification. *Sensors* **2015**, *15*, 13110−13120.
(44) Wang, L.; Major, D.; Paga, P.; Zhang, D.; Norton, M. G.; McIlroy, D. N. High yield synthesis and lithography of silica-based nanospring mats. *Nanotechnology* **2006**, *17*, S298−S303.
(45) Wojcik, P. M.; Bakharev, P. V.; Corti, G.; McIlroy, D. N. Nucleation, evolution, and growth dynamics of amorphous silica nanosprings. *Mater. Res. Express* **2017**, *4*, 015004.
(46) Korotcenkov, G.; Brinzari, V.; Ivanov, M.; Cerneavschi, A.; Rodriguez, J.; Cirera, A.; Cornet, A.; Morante, J. Structural stability of indium oxide films deposited by spray pyrolysis during thermal annealing. *Thin Solid Films* **2005**, *479*, 38−51.
(47) Zhu, Y.; Zhang, X.; Li, R.; Li, Q. Planar-defect-rich zinc oxide nanoparticles assembled on carbon nanotube films as ultraviolet emitters and photocatalysts. *Sci. Rep.* **2015**, DOI: 10.1038/srep04728.
(48) Binner, J.; Wang, J.; Vaidhyanathan, B.; Joomun, N.; Kilner, J.; Dimitrakis, G.; Cross, T. E. Evidence for the microwave effect during the annealing of zinc oxide. *J. Am. Ceram. Soc.* **2007**, *90*, 2693−2697.

DOI: 10.1021/acssensors.8b00746
ACS Sens. 2018, 3, 2367−2374

(49) Dobrokhotov, V.; Oakes, L.; Sowell, D.; Larin, A.; Hall, J.; Kengne, A.; Bakharev, P.; Corti, G.; Cantrell, T.; Prakash, T.; Williams, J.; McIlroy, D. N. ZnO coated nanospring-based chemiresistors. *J. Appl. Phys.* **2012**, *111*, 044311.
(50) Dobrokhotov, V.; McIlroy, D. N.; Norton, M. G.; Abuzir, A.; Yeh, W. J.; Stevenson, I.; Pouy, R.; Bochenek, J.; Cartwright, M.; Wang, L.; Dawson, J.; Beaux, M.; Berven, C. Principles and mechanisms of gas sensing by GaN nanowires functionalized with gold nanoparticles. *J. Appl. Phys.* **2006**, *99*, 104302.
(51) Bakharev, P.; Dobrokhotov, V.; McIlroy, D. N. A Method for Integrating ZnO Coated Nanosprings into a Low Cost Redox-Based Chemical Sensor and Catalytic Tool for Determining Gas Phase Reaction Kinetics. *Chemosensors* **2014**, *2*, 56−68.
(52) Kirkpatrick, S. Percolation and Conduction. *Rev. Mod. Phys.* **1973**, *45*, 574−588.
(53) Bunde, A.; Dieterich, W. Percolation in Composites. *J. Electroceram.* **2000**, *5*, 81−92.
(54) Tremblay, A.-M.; Machta, J. Finite-size effects in continuum percolation. *Phys. Rev. B: Condens. Matter Mater. Phys.* **1989**, *40*, 5131−5139.
(55) Kumar, S.; Murthy, J.; Alam, M. Percolating Conduction in Finite Nanotube Networks. *Phys. Rev. Lett.* **2005**, DOI: 10.1103/PhysRevLett.95.066802.
(56) Martin, J.; Anderson, R.; Odinek, J.; Adolf, D.; Williamson, J. Controlling percolation in field-structured particle composites: Observations of giant thermoresistance, piezoresistance, and chemiresistance. *Phys. Rev. B: Condens. Matter Mater. Phys.* **2003**, DOI: 10.1103/PhysRevB.67.094207.

DOI: 10.1021/acssensors.8b00746
ACS Sens. 2018, 3, 2367−2374